

# Left-right twin Higgs model confronted with the latest LHC Higgs data

Yao-Bei Liu<sup>1,2</sup>, Shan Cheng<sup>1</sup>, Zhen-Jun Xiao<sup>1</sup> <sup>a</sup>

1. *Department of Physics and Institute of Theoretical Physics,  
Nanjing Normal University, Nanjing, Jiangsu 210023, P.R.China*

2. *Henan Institute of Science and Technology, Xinxiang 453003, P.R.China*

(Dated: October 12, 2018)

Motivated by the latest LHC Higgs data, we calculate the new physics contributions to the Higgs decay channels of  $h \rightarrow \gamma\gamma, Z\gamma, \tau\tau, WW^*$  and  $ZZ^*$  in the left-right twin Higgs (LRTH) model, induced by the loops involving the heavy T-quark, the  $W_H$  and  $\phi^\pm$  bosons appeared in the LRTH model. We find that (a) for a SM-like Higgs boson around 125.5 GeV, the signal rates normalized to the corresponding standard model (SM) predictions are always suppressed when new physics contributions are taken into account and approach the SM predictions for a large scalar parameter  $f$ ; and (b) the LRTH prediction for  $R_{\gamma\gamma}$  agree well with the CMS measurement  $R_{\gamma\gamma} = 0.77 \pm 0.27$  at  $1\sigma$  level, but differ with the ATLAS result. The forthcoming precision measurement of the diphoton signal at the LHC can be a sensitive probe for the LRTH model.

PACS numbers: 12.60.Fr, 14.80.Cp, 14.70.Bh

arXiv:1311.0183v3 [hep-ph] 28 Jan 2014

---

<sup>a</sup> Electronic address: xiaozhenjun@njnu.edu.cn

## I. INTRODUCTION

Very Recently, the discovery of a neutral Higgs boson at CERN's Large Hadron Collider (LHC) experiment has been confirmed by the ATLAS and CMS collaborations [1–6]. This discovery is based on the Higgs boson search with a variety of Higgs boson decay modes. Among the major decay modes of a standard model (SM) Higgs boson studied intensively at ATLAS and CMS experiments, the diphoton channel is one of the most important channels for Higgs searches and studies of its properties at the LHC experiments due to its high resolution, small background and a clear discrepancy between the measured signal strength as reported by ATLAS [5, 6] and CMS Collaboration [4]:

$$R_{\gamma\gamma} = 1.55 \pm 0.23(stat) \pm 0.15(syst), \quad (ATLAS), \quad (1)$$

$$R_{\gamma\gamma} = 0.77 \pm 0.27 \quad (CMS). \quad (2)$$

Both measurements are still consistent with the SM prediction ( $R_{\gamma\gamma} = 1$ ) in the  $2\sigma$  range at present due to still large errors. If the excess (deficit) seen by ATLAS (CMS) is eventually confirmed by the near future LHC measurements, the extra contributions from various new physics (NP) models beyond the SM maybe help to understand such excess or deficit. Of course, all extensions of the SM have to abide by the existence of a Higgs boson with mass of about 125 GeV and with SM-like properties.

The twin Higgs mechanism has been proposed as an alternative solution to the little hierarchy problem [7, 8]. The idea of twin Higgs shares the same origin with that of little Higgs in that the SM-like Higgs emerges as a pseudo-Goldstone boson [9]. But rather than using collective symmetry breaking, the twin Higgs mechanism takes an additional discrete symmetry to stabilize the Higgs mass. The twin Higgs mechanism can be implemented in left-right Higgs (LRTH) model with the discrete symmetry being identified with left-right symmetry [8]. The phenomenology of the LRTH model has been extensively studied for example in Refs. [10–12].

The LHC diphoton signal has been studied in various new physics models, such as some popular supersymmetry models [13], the two Higgs doublet model [14], the Higgs triplet model [15], the models with extra-dimensions [16], the little Higgs models [17], and the other extensions of Higgs models [18, 19]. In the LRTH model, the diphoton decay of the SM-like Higgs boson was studied even before the LHC Higgs data [20]. In this work, motivated by the latest LHC discrepancy of  $R_{\gamma\gamma}$ , we will assume a SM-like Higgs boson with 125.5 GeV mass and study its implication in the LRTH model. Also we will study some exclusive signal rates compared with the Higgs data as well as the SM predictions. Besides, we will perform a global fit to the latest LHC Higgs data to figure out if the LRTH model can provide a better fit than the SM.

This paper is organized as follows. In the next section, we recapitulate the LRTH model and lay out the couplings of the particles relevant to our calculation. In Sec. III, we investigate the LRTH model predictions for the Higgs signal rates in light of the latest LHC experimental data. Finally, we give our conclusion in Sec.IV.

## II. RELEVANT HIGGS COUPLINGS IN THE LRTH MODEL

The LRTH model is based on the global symmetry  $U(4) \times U(4)$  with a locally gauged  $SU(2)_L \times SU(2)_R \times U(1)_{B-L}$  subgroup. The twin symmetry is identified as the left-right symmetry which interchanges L and R, implying that the gauge couplings of  $SU(2)_L$  and  $SU(2)_R$  are identical ( $g_{2L} = g_{2R}$ ). Two Higgs fields,  $H$  and  $\hat{H}$ , are introduced and each transforms as  $(4, 1)$  and  $(1, 4)$

respectively under the global symmetry, which can be written as

$$H = \begin{pmatrix} H_L \\ H_R \end{pmatrix}, \quad \hat{H} = \begin{pmatrix} \hat{H}_L \\ \hat{H}_R \end{pmatrix}, \quad (3)$$

where  $H_{L,R}$  and  $\hat{H}_{L,R}$  are two component objects which are charged under the  $SU(2)_L \times SU(2)_R \times U(1)_{B-L}$  as

$$H_L \text{ and } \hat{H}_L : (2, 1, 1), \quad H_R \text{ and } \hat{H}_R : (1, 2, 1). \quad (4)$$

The global  $U(4)_1(U(4)_2)$  symmetry is spontaneously broken down to its subgroup  $U(3)_1(U(3)_2)$  with non-zero vacuum expectation values(VEV) as

$$\langle H \rangle = \begin{pmatrix} 0 \\ 0 \\ 0 \\ f \end{pmatrix}, \quad \langle \hat{H} \rangle = \begin{pmatrix} 0 \\ 0 \\ 0 \\ \hat{f} \end{pmatrix}. \quad (5)$$

The Higgs VEVs also break  $SU(2)_R \times U(1)_{B-L}$  down to the SM  $U(1)_Y$ . The details of the LRTH model as well as the gauge sector, the fermion sector and Higgs sector have been given in Ref.[10]. Here we will focus on the new particles and the couplings relevant to our work.

In the LRTH model, the heavy new gauge bosons ( $W_H^\pm, Z_H$ ), heavy top quark partner ( $T$ ) and other Higgs particles ( $\phi^{0,\pm}$ ) are introduced to cancel the Higgs boson one-loop quadratic divergence contributed by the gauge bosons, top quark and Higgs boson of the SM. The masses of the particles that run in the triangle loop diagrams are given in Ref. [10]. The relevant Higgs couplings and the mixing angles for left-handed and right-handed fermions are the following [10]

$$\begin{aligned} \mathcal{L} = & -\frac{m_t}{v} y_t \bar{t} t h - \frac{m_T}{v} y_T \bar{T} T h + 2 \frac{m_W^2}{v} y_W W^+ W^- h \\ & + 2 \frac{m_{W_H}^2}{v} y_{W_H} W_H^+ W_H^- h + 2 \frac{m_Z^2}{v} y_Z Z Z h - 2 \frac{m_\phi^2}{v} y_\phi \phi^+ \phi^- h, \end{aligned} \quad (6)$$

$$s_L = \frac{1}{\sqrt{2}} \sqrt{1 - (y^2 f^2 \cos 2x + M^2)/N_t}, \quad (7)$$

$$s_R = \frac{1}{\sqrt{2}} \sqrt{1 - (y^2 f^2 \cos 2x - M^2)/N_t}, \quad (8)$$

where  $N_t = \sqrt{(M^2 + y^2 f^2)^2 - y^4 f^4 \sin^2 2x}$  with  $x = v/\sqrt{2}f$  and  $v = 246\text{GeV}$  is the electroweak scale, while  $M$  is the mass parameter essential to the mixing between the SM-like top quark and the heavy top quark. The explicit expressions of the relevant couplings  $y_t, y_T, y_W, y_{W_H}$  and  $y_\phi$  can be found easily in Ref. [10].

In the LRTH model, the relation between  $G_F$  and  $v$  is modified from its SM form, introducing an additional correction  $y_{G_F}$  as  $1/v^2 = \sqrt{2}G_F y_{G_F}^2$  with  $y_{G_F}^2 = 1 - v^2/(6f^2)$ . This correction must also be taken into account when comparing SM-like Higgs boson decay rates (i.e.  $h \rightarrow XX$ ) in the LRTH model to the SM predictions with  $G_F$  as input.

### III. HIGGS DECAYS IN THE LRTH MODEL

#### A. The rates of $\sigma(gg \rightarrow h \rightarrow XX)$ at the LHC

The Higgs production rates in the LRTH model normalized to the SM values are generally defined as

$$R_{XX} = \frac{\sigma(pp \rightarrow h)Br(h \rightarrow XX)}{\sigma_{SM}(pp \rightarrow h)Br_{SM}(h \rightarrow XX)}, \quad (9)$$

where  $XX$  denotes  $\gamma\gamma$ ,  $Z\gamma$ ,  $ZZ^*$ ,  $WW^*$ , or the SM fermion pairs.

At the LHC, the Higgs single production is dominated by the gluon-gluon fusion process. The hadronic cross section  $\sigma(gg \rightarrow h)$  at leading order can be written as:

$$\sigma(gg \rightarrow h) = \frac{\pi^2 \tau_0}{8m_h^3} \Gamma(h \rightarrow gg) \int_{\tau_0}^1 \frac{dx}{x} f_g(x, \mu_F^2) f_g\left(\frac{\tau_0}{x}, \mu_F^2\right), \quad (10)$$

where  $\tau_0 = m_h^2/s$  with  $\sqrt{s}$  being the center-of-mass energy of the LHC and  $f_g(x, \mu_F^2)$  is the parton distribution of gluon. Thus, one can see that the  $\sigma(gg \rightarrow h)$  has a strong correlation with the decay width  $\Gamma(h \rightarrow gg)$ . Other main production processes of the Higgs boson include vector-boson fusion (VBF), and associated production with SM gauge bosons (VH) and top pair  $t\bar{t}h$ . For  $m_h = 125.5$  GeV, the uncertainty on Higgs production has been studied systematically by the LHC Higgs cross section working group for the various channels and can be found easily in Ref. [21]. The major decay modes of the Higgs boson are  $h \rightarrow f\bar{f}$  ( $f = b, c, \tau$ ),  $VV^*$  ( $V = W, Z$ ),  $gg$ ,  $\gamma\gamma$  and  $Z\gamma$ , where  $W^*/Z^*$  denoting the off-shell charged or neutral electroweak gauge bosons. The corresponding expressions are given in the Appendix.

The SM input parameters relevant in our study are taken from [22]. The free LRTH model parameters involved are  $f$ ,  $M$ , and the masses of the charged Higgs bosons. The indirect constraints on  $f$  come from the  $Z$ -pole precision measurements, the low energy neutral current process and high energy precision measurements off the  $Z$ -pole, requiring approximately  $f > 500$  GeV. On the other hand, it cannot be too large since the fine tuning is more severe for large  $f$ . The mixing parameter  $M$  is constrained by the  $Z \rightarrow b\bar{b}$  branching ratio and oblique parameters. Following Ref. [10], we take the typical parameter space as:

$$500\text{GeV} \leq f \leq 1500\text{GeV}, \quad 0 \leq M \leq 150\text{GeV}, \quad (11)$$

while the mass  $m_\phi$  of the charged Higgs boson  $\phi^\pm$  is in the range of a few hundred GeV.

For the considered  $h \rightarrow XX$  decays, one can write the decay amplitude  $\mathcal{A}(h \rightarrow XX)$  as the summation of the pieces  $\mathcal{A}_i$  from different sources:

$$\mathcal{A}(h \rightarrow XX) = \sum_{i=1}^N \mathcal{A}_i(h \rightarrow XX). \quad (12)$$

In Table I, we list all possible contributions to the decay amplitude  $\mathcal{A}(h \rightarrow \gamma\gamma)$  and  $\mathcal{A}(h \rightarrow gg)$  coming from various sources, here we show the relative strength of different pieces only.

For the  $h \rightarrow \gamma\gamma$  decay, for example, the SM contribution include two parts: one comes from the top quark loop with  $\mathcal{A}_{top} = -1.84$ , another from the  $W^\pm$  boson with  $\mathcal{A}_W = 8.34$ . These two contributions have different sign and therefore interfere destructively. In the LRTH model, however, the Feynman diagrams involving the  $T$ -quark,  $W_H$  boson and  $\phi^\pm$  boson also provide the additional contributions to the decay  $h \rightarrow \gamma\gamma$  respectively, as illustrated explicitly in the column four to six of Table I. From Table I we have the following observations:

TABLE I. The relative strength of the contributions to the decay amplitude from various sources for  $h \rightarrow \gamma\gamma$  and  $h \rightarrow gg$  (numbers in the brackets) in the SM and the LRTH model, assuming  $m_\phi = 200$  GeV,  $M = 150$  GeV and  $f = 500, 700, 900, 1100, 1500$  GeV, respectively.

$m_h=125.5$ GeV	SM top	$W^\pm$	T-quark	$W_H$	$\phi^\pm$	total
SM	-1.84 (0.69)	8.34 (0)	0	0	0	6.50 (0.69)
$f=500$ GeV	-1.68 (0.63)	7.84 (0)	0.18 (-0.07)	-0.031	-0.009	6.31 (0.56)
$f=700$ GeV	-1.77 (0.66)	8.08 (0)	0.10 (-0.04)	-0.016	-0.004	6.40 (0.62)
$f=900$ GeV	-1.79 (0.67)	8.19 (0)	0.06 (-0.024)	-0.01	-0.003	6.44 (0.65)
$f=1100$ GeV	-1.81 (0.68)	8.24 (0)	0.04 (-0.016)	-0.007	-0.002	6.46 (0.66)
$f=1500$ GeV	-1.82 (0.68)	8.28 (0)	0.02 (-0.01)	-0.004	-0.001	6.48 (0.67)

1. In the SM, the decay  $h \rightarrow gg$  is dominated by the top quark loop, while the contributions to  $h \rightarrow \gamma\gamma$  arise from both the top quark and  $W$  boson loops simultaneously. The total decay amplitude of  $h \rightarrow \gamma\gamma$  is clearly dominated by the large positive contribution from the SM  $W^\pm$  bosons loop.
2. In the LRTH model, the additional new physics contributions are indeed much smaller in size than the SM part and therefore play a minor role for the considered decay modes.
3. Among the three NP sources, the contribution from the T-quark is the largest piece of the NP contributions, but it is still too small to counteract with the positive SM part, this is because the coupling  $y_T$  is much smaller than  $y_t$ . The NP contributions from  $W_H$  and  $\phi^\pm$  are even much smaller than the small T-quark piece and can be neglected safely.
4. The NP contributions become smaller rapidly when  $f$  becomes larger. For  $h \rightarrow \gamma\gamma$  decay, for example, the contribution from the T-quark is changing from 0.18 to 0.02 when the parameter  $f$  increases from 500 GeV to 1500 GeV.

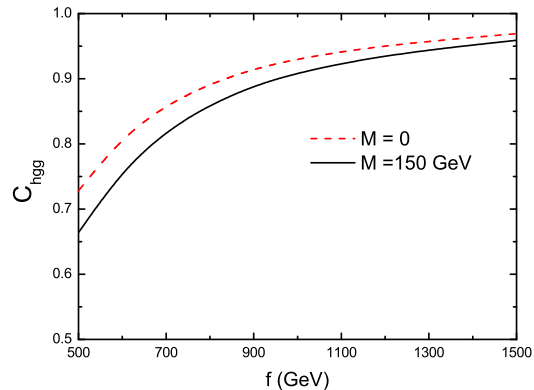


FIG. 1.  $f$ -dependence of the ratio  $C_{hgg}$  for two typical values of  $M$  as indicated.

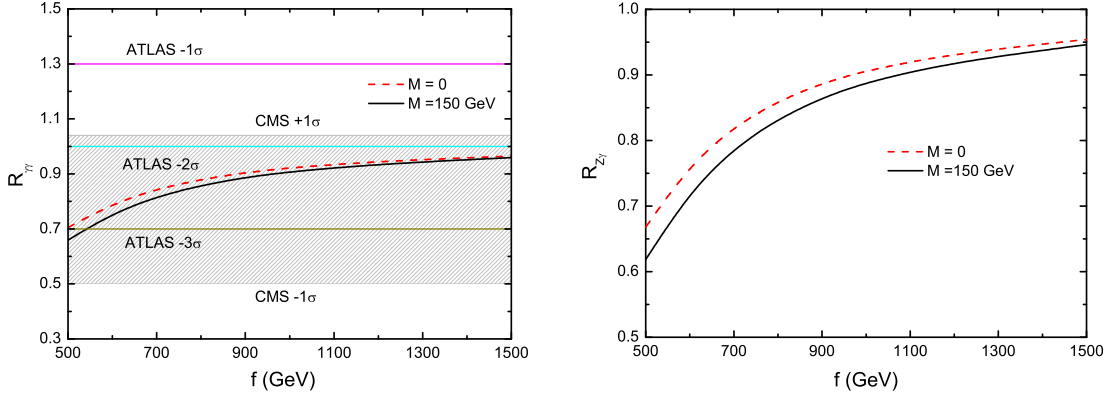


FIG. 2.  $f$ -dependence of  $R_{\gamma\gamma}$  (left) and  $R_{Z\gamma}$  (right) for two typical values of  $M$  as indicated. The shaded area shows the CMS result:  $R_{\gamma\gamma} = 0.77 \pm 0.27$ .

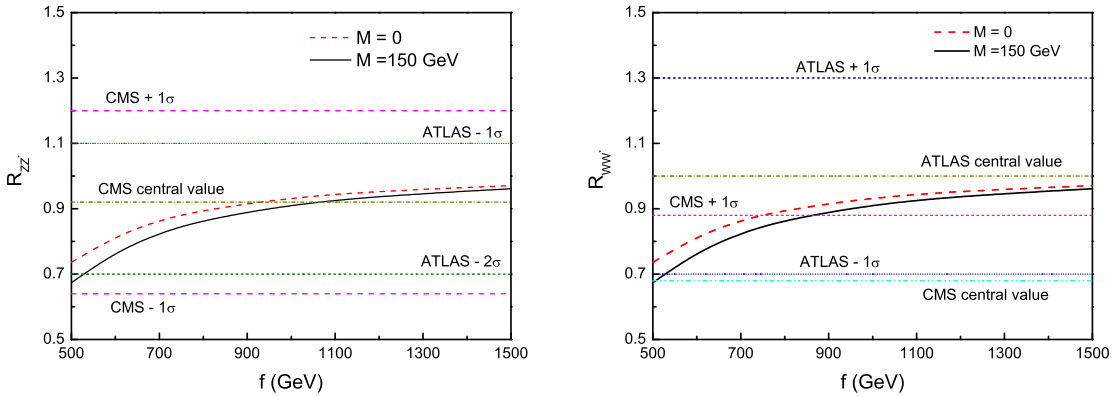


FIG. 3.  $f$ -dependence of  $R_{ZZ^*}$  (left) and  $R_{WW^*}$  (right) for two typical values of  $M$  as indicated.

In Fig.1 we show the  $f$ -dependence of the ratios  $C_{hgg} = \Gamma_{LRTH}(h \rightarrow gg)/\Gamma_{SM}(h \rightarrow gg)$  for two typical values of  $M$ :  $M = 0, 150$  GeV. Here  $\Gamma_{SM}(h \rightarrow gg)$  denotes the decay width of  $h \rightarrow gg$  in the SM. One can see that the NP correction becomes smaller rapidly along with the increase of the parameter  $f$ , but becomes larger when  $M$  is increasing. This is because the parameter  $M$  is introduced to generate the mass mixing term  $M_{qL}q_R$ , and the LRTH model can give corrections via the coupling of  $ht\bar{t}$  and the heavy  $T$ -quark loop. For the special case of  $M = 0$ , there is no mixing between the SM top quark and the heavy  $T$  quark. By assuming  $f = 500$  GeV and varying  $M$  in the range of  $0 \leq M \leq 150$  GeV, the NP correction can be changed from 17% to the SM value.

We know that the large experimental and theoretical uncertainties may prevent the detection of the deviation of the LRTH model prediction of  $C_{hgg}$  from the SM one for large value of scale  $f$ . The QCD corrections to the total cross section of  $h \rightarrow gg$  have been computed at next-to-

next-to-leading order (NNLO) in Ref. [23]. The remaining renormalization/factorization scale dependence of the cross section gives a lower bound on the size of the theoretical uncertainty due to uncalculated higher-order QCD radiative corrections of about 15% [24], which can be further reduced with the inclusion of recently known NNNLO results as described in Ref. [25].

In Fig.2 we plot the ratio  $R_{\gamma\gamma}$  and  $R_{Z\gamma}$  versus  $f$  for two typical values of  $M$  in the LRTH model. It can be seen from Fig.2 that the ratio  $R_{\gamma\gamma}$  and  $R_{Z\gamma}$  in the LRTH model are always smaller than unit, and will approach one for a large  $f$ . On the other hand, for a small value of parameter  $f$ , the deviation from the SM prediction is sensitive to the mixing parameter  $M$ .

For the diphoton signal, the measured value of  $R_{\gamma\gamma} = 0.77 \pm 0.27$  as reported by CMS Collaboration can be understood in the LRTH model. Of course, the LRTH prediction for  $R_{\gamma\gamma}$  is always outside  $2\sigma$  range of the ATLAS result. The key point here is the large difference between the central values of the measured  $R_{\gamma\gamma}$  as reported by ATLAS and CMS Collaborations. Further improvement of the  $R_{\gamma\gamma}$  measurements for both ATLAS and CMS Collaboration is greatly welcome and will play the key role in constraining the new physics models beyond the SM.

For the  $h \rightarrow Z\gamma$  channel there is not enough data to draw any conclusion about LRTH. For the ratios  $R_{ZZ^*}$  and  $R_{WW^*}$ , the ATLAS and CMS measurements are consistent with each other within one standard deviation. In Fig.3 we plot the  $f$ -dependence of the ratio  $R_{ZZ^*}$  and  $R_{WW^*}$  for two typical values of  $M$ . It can be seen from Fig.3 that the ratio  $R_{ZZ^*}$  and  $R_{WW^*}$  in the LRTH model are always smaller than unit and sensitive to the value of parameter  $f$  and  $M$ .

TABLE II. The theoretical predictions for the Higgs production rates  $R_{XX}$  in the LRTH model, assuming  $m_\phi=200$  GeV,  $M=150$  GeV and  $f = 500, 800, 1200$  and  $1500$  GeV. The corresponding measured values reported by ATLAS and CMS [4–6] are listed as comparison.

$f$ (GeV)	$R_{\gamma\gamma}$	$R_{ZZ^*}$	$R_{WW^*}$	$R_{\tau^+\tau^-}$	$R_{Z\gamma}$
500	0.659	0.674	0.674	0.674	0.619
800	0.858	0.866	0.866	0.866	0.833
1200	0.936	0.939	0.939	0.939	0.92
1500	0.959	0.961	0.961	0.961	0.946
ATLAS	$1.55 \pm 0.23 \pm 0.15$	$1.43 \pm 0.33 \pm 0.17$	$0.99 \pm 0.21 \pm 0.21$	$0.7 \pm 0.7$	$< 13.5$
CMS	$0.77 \pm 0.27$	$0.92 \pm 0.28$	$0.68 \pm 0.2$	$1.1 \pm 0.41$	$< 9.3$

In Table II, we list the LRTH predictions for the Higgs boson production rates  $R_{\gamma\gamma}$ ,  $R_{WW^*}$ ,  $R_{ZZ^*}$ ,  $R_{\tau\tau}$  and  $R_{Z\gamma}$ , assuming  $M = 150\text{GeV}$ ,  $m_\phi = 200$  GeV and  $500 \leq f \leq 1500$  GeV. From the numerical results as listed in Table II, one can see the five signal rates are always suppressed when the new physics contributions are taken into account, which is similar with the situation in the little Higgs models [26]. This is mainly due to the following common reasons in these kind of new physics models:

1. The couplings of top quark partner  $T$  and new heavy gauge bosons  $W_H$  with the Higgs boson have the opposite sign with respect to the Higgs couplings with SM top quark and gauge bosons, respectively.
2. The new physics part of the Higgs couplings to the SM top quark and gauge bosons are suppressed by the ratio  $v^2/f^2$ , and will become zero in the limit  $f \rightarrow \infty$ .

It is well known that the production and decays of the Higgs boson are largely affected by high order corrections. In order to reduce the errors of theoretical predictions, we defined  $R_{XX}$  as the ratios of the theoretical predictions in the SM and in the LRTH model. In this way, the theoretical errors will be largely canceled.

In many cases, the higher order corrections to the relevant cross sections or the branching ratios could be factorized out approximately as simple factors (NLO, or NNLO, etc) of the leading order results as discussed in Ref. [27]. For instance, one can see that the NLO QCD corrections to both  $hgg$  and  $h\gamma\gamma$  vertex can give a simple multiplicative factor. We assume that the QCD corrections in the LRTH model are similar as those in the SM top loop for simplicity, thus the QCD corrections cancel to a large extent in these ratios, provided that a single production mechanism dominates. This certainly applies to  $\mu_{\gamma\gamma}$ ,  $\mu_{VV}$ , and  $\mu_{\tau+\tau-}$  which are governed by the dominant production channel through gluon fusion [28].

## B. Global fit of the LRTH model to current LHC Higgs data

By using the latest LHC Higgs data of 17 channels from both ATLAS and CMS as given in Refs. [29, 30], we now perform a global fit to the LRTH model with the method proposed in [28, 31]. When fitting the various observables, we consider the correlation coefficients given in Ref.[32] due to the independent data for different exclusive search channels by two collaborations.

The global  $\chi^2$  function is defined as usual:

$$\chi^2 = \sum_{i,j} (\mu_i - \hat{\mu}_i)(\sigma^2)_{ij}^{-1}(\mu_j - \hat{\mu}_j), \quad (13)$$

where index  $i, j$  runs over all the different production/decay channels considered in this paper,  $(\mu_i, \mu_j)$  and  $(\hat{\mu}_i, \hat{\mu}_j)$  are the corresponding theoretical signal strength in the LRTH model and the measured Higgs signal strengths as reported by both ATLAS and CMS collaborations, respectively.  $\sigma_{ij}^2 = \sigma_i \rho_{ij} \sigma_j$ ,  $\sigma$  is the experimental error extracted from the data at  $1\sigma$  and  $\rho_{ij}$  is the correlation matrix. Taking two correlated observables for instance, the correlation coefficient  $\rho$  is applicable to the following formula

$$\chi_{1,2}^2 = \frac{1}{(1 - \rho^2)} \cdot \left[ \frac{[\mu_1 - \hat{\mu}_1]^2}{\sigma_1^2} + \frac{[\mu_2 - \hat{\mu}_2]^2}{\sigma_2^2} - 2\rho \frac{[\mu_1 - \hat{\mu}_1] \cdot [\mu_2 - \hat{\mu}_2]}{\sigma_1 \sigma_2} \right]. \quad (14)$$

Note that the errors on the reported Higgs signal strengths  $\hat{\mu}_i$  are symmetrized by the relation

$$\delta \hat{\mu}_i = \sqrt{[(\delta \hat{\mu}_+)^2 + (\delta \hat{\mu}_-)^2]/2}, \quad (15)$$

where  $\delta \hat{\mu}_{\pm}$  are the one-sided errors given by the experimental collaborations. For plotting distributions of a function of one variable, the 68% ( $1\sigma$ ) and 95% ( $2\sigma$ ) confidence level (CL) intervals are obtained by  $\chi^2 = \chi_{min}^2 + 1$  and  $+4$ , respectively. For a more detailed description of the fit procedure, one can see Refs. [28, 31, 32].

In Fig. 4 we project the samples on the global fit values of  $\chi^2$  versus parameter  $f$  for  $M = 0$  and 150 GeV. One can see that the value of  $\chi^2$  is larger than that for SM for most of parameter space of  $f$  and approaches the SM value for a sufficiently large  $f$ . For a large values of scale  $f$  (about 1100 GeV), it is slightly smaller than the SM value ( $\chi^2 = 14.88$  for  $M = 150$  GeV while  $\chi_{SM}^2 = 14.89$ ). So we can see that the good points favored by the current LHC Higgs data is at the region of  $f \geq 1100$  GeV. For  $M = 150$  GeV and  $f < 550$  GeV, the value of  $\chi^2$  is larger than



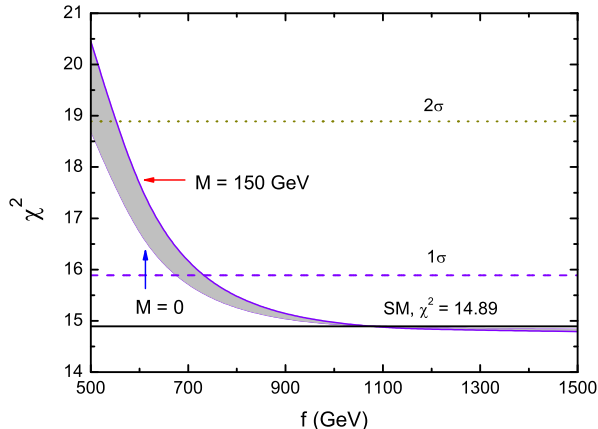


FIG. 4. The global fit values of  $\chi^2$  versus  $f$  for  $M = 0$  and 150 GeV.

18.9, which implies that  $f < 550$  GeV is excluded at 95% confidence level from the experimental viewpoint

In Fig.5 we present the LRTH predictions of different Higgs signal rates  $R_{XX}$ , and a comparison with the corresponding experimental measurements at the LHC, assuming  $M = 150$  GeV and the scalar parameter  $f = 500, 800$  and  $1200$  GeV respectively. In our fit, we select 17 sets of data from Refs.[29, 30]. From Fig.5 one can see that all the signal rates are suppressed due to the inclusion of new physics corrections in the LRTH model, when compared with the SM values. In the LRTH model, we find  $\chi^2 = 20.29, 15.39, 14.82$  for  $f = 500, 800$  and  $1200$  GeV. The LRTH prediction for  $R_{\gamma\gamma}$  agree well with the CMS measurement:  $R_{\gamma\gamma}^{\text{CMS}} = 0.77 \pm 0.27$ .

For given values of the LRTH parameter  $M$  and  $f$ , the masses  $M_T, M_{W_H}$  and the relevant couplings  $y_t, y_T$  and  $y_W$  will be determined consequently. In Table III we present the numerical results of the LRTH predictions for some ratios and various Higgs signal rates, as illustrated explicitly in Fig. 5.

In the near future, the improved measurement of the diphoton signal at the LHC will play a decisive role for these models. For example, if the future well-measured diphoton rate is still clearly larger than unit, the LRTH model and other little Higgs models will be strongly disfavored or ruled out. Otherwise, if the deficit signal rate permits, these models will be favored. However, it is difficult for the LHC to clearly discriminate these new physics models due to the different free parameters for each model. The high energy and high luminosity linear electron positron collider experiments, such as CLIC or the ILC, will provide a rather clean environment for new physics discovery [33].

#### IV. CONCLUSIONS

In this work, we studied the Higgs production and decay in the LRTH model in the light of the latest LHC Higgs data from ATLAS and CMS Collaboration. From the numerical results we obtain the following observations:

1. The signal rates normalized to the SM prediction for the five Higgs search channels are

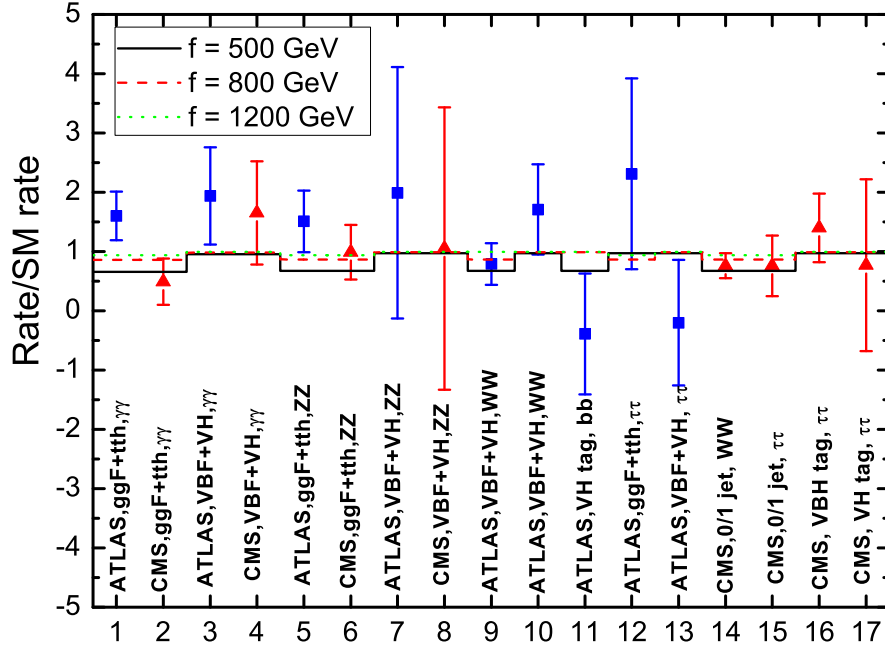


FIG. 5. The LRTM predictions for the various Higgs signal rates  $R_{XX}$  at the LHC, assuming  $M = 150$  GeV,  $f = 500, 800$  and  $1200$  GeV respectively. The error-bars show the ATLAS and CMS measurements of 17 channels as given in Refs. [29, 30].

always suppressed when new physics contributions are taken into account and approach the SM predictions for a large scale parameter  $f$ .

2. The LRTM prediction for  $R_{\gamma\gamma}$  agree well with the CMS measurement at  $1\sigma$  level, but differ with the ATLAS result. The LRTM model could be further tested by the improved measurement of  $R_{\gamma\gamma}$  at LHC.

## ACKNOWLEDGMENTS

This work is supported by the National Natural Science Foundation of China under the Grant No. 11235005 and the Joint Funds of the National Natural Science Foundation of China (U1304112).

## Appendix A: The Higgs decays in the LRTM model

In the LRTM model, the decays  $h \rightarrow gg, \gamma\gamma, Z\gamma$  all receive contributions from the modified couplings  $hXX$  and the new heavy particles. The LO decay widths of  $h \rightarrow gg, \gamma\gamma, Z\gamma$  are given

TABLE III. The numerical results of the LRTH predictions for some ratios and various Higgs signal rates, assuming  $M = 0, 150$  and  $f = 500, 800$  GeV, respectively.

$M$ (GeV)	0		150	
$f$ (GeV)	500	800	500	800
$m_T$ (GeV)	464.9	774.4	488.5	788.8
$m_{W_H}$ (GeV)	1175.6	1883.7	1175.6	1883.9
$y_t^2$	1.0	1.0	0.871	0.959
$y_T^2$	0.017	0.002	0.011	0.002
$y_W^2$	0.921	0.969	0.921	0.969
$C_{hgg}$	0.728	0.892	0.664	0.861
$C_{h\gamma\gamma}$	0.919	0.966	0.939	0.976
$C_{hZ\gamma}$	0.871	0.944	0.881	0.947
$C_{hVV^*}$	0.921	0.969	0.921	0.969
ggF+ttH, $\gamma\gamma$	0.705	0.882	0.663	0.858
VBF+VH, $\gamma\gamma$	0.931	0.971	0.953	0.982
ggF+ttH, $ZZ$	0.736	0.896	0.674	0.866
VBF+VH, $ZZ$	0.971	0.989	0.974	0.989
ggF+ttH, $WW$	0.736	0.896	0.674	0.866
VBF+VH, $WW$	0.971	0.989	0.974	0.989
VH tag, $b\bar{b}$	0.971	0.989	0.974	0.989
ggF+ttH, $\tau\tau$	0.736	0.896	0.674	0.866
VBF+VH, $\tau\tau$	0.971	0.989	0.974	0.989
0/1 jet, $WW$	0.973	0.897	0.674	0.866
0/1 jet, $\tau\tau$	0.941	0.898	0.681	0.868
VBF tag, $\tau\tau$	0.998	0.999	1.000	1.001
VH tag, $\tau\tau$	0.971	0.989	0.974	0.989
$\chi^2$	18.55	15.19	20.3	15.39

by

$$\Gamma(h \rightarrow gg) = \frac{\sqrt{2}G_F\alpha_s^2 m_h^3}{32\pi^3} \left| -\frac{1}{2}F_{1/2}(\tau_t)y_t y_{G_F} - \frac{1}{2}F_{1/2}(\tau_T)y_T \right|^2, \quad (\text{A1})$$

$$\Gamma(h \rightarrow \gamma\gamma) = \frac{\sqrt{2}G_F\alpha_e^2 m_h^3}{256\pi^3} \left| \frac{4}{3}F_{1/2}(\tau_t)y_t y_{G_F} + \frac{4}{3}F_{1/2}(\tau_T)y_T \right. \\ \left. + F_1(\tau_W)y_W + F_1(\tau_{W_H})y_{W_H} + F_0(\tau_\phi)y_\phi \right|^2, \quad (\text{A2})$$

$$\Gamma(h \rightarrow Z\gamma) = \frac{\alpha_e^2 m_h^3}{128\pi^3 s_W^2 c_W^2 v^2} (1 - m_Z^2/m_h^2)^3 \\ \cdot \left| 2y_f(1 - \frac{8}{3}s_W^2)A_{1/2}(\tau_f, \lambda_f) + y_W c_W^2 A_1(\tau_W, \lambda_W) \right|^2, \quad (\text{A3})$$

with

$$\begin{aligned}
F_1 &= 2 + 3\tau + 3\tau(2 - \tau)f(\tau), \\
F_{1/2} &= -2\tau[1 + (1 - \tau)f(\tau)], \\
F_0 &= \tau[1 - \tau f(\tau)], \\
A_1 &= 4(3 - \tan^2 \theta_W)I_2(\tau, \lambda) + (1 + 2\tau^{-1}) \tan^2 \theta_W - (5 + 2\tau^{-1})I_1(\tau, \lambda), \\
A_{1/2} &= I_1(\tau, \lambda) - I_2(\tau, \lambda),
\end{aligned} \tag{A4}$$

where

$$I_1(\tau, \lambda) = \frac{\tau\lambda}{2(\tau - \lambda)} + \frac{\tau^2\lambda^2}{2(\tau - \lambda)^2}[f(\tau) - f(\lambda)] + \frac{\tau^2\lambda}{(\tau - \lambda)^2}[g(\tau) - g(\lambda)], \tag{A5}$$

$$I_2(\tau, \lambda) = -\frac{\tau\lambda}{2(\tau - \lambda)}[f(\tau) - f(\lambda)], \tag{A6}$$

with

$$\begin{aligned}
f(\tau) &= [\sin^{-1}(1/\sqrt{\tau})]^2, \\
g(\tau) &= \sqrt{\tau - 1} \sin^{-1}(1/\sqrt{\tau}),
\end{aligned} \tag{A7}$$

for  $\tau_i = 4m_i^2/m_h^2 \geq 1$ .

The partial decay widths into single off-shell gauge bosons  $h \rightarrow VV^*$  are given in Ref. [34]

$$\Gamma(h \rightarrow WW^*) = \frac{3G_F^2 m_W^4 m_h}{16\pi^3} F\left(\frac{m_W^2}{m_h^2}\right), \tag{A8}$$

$$\Gamma(h \rightarrow ZZ^*) = \left(\frac{7}{4} - \frac{10}{3}s_W^2 + \frac{40}{9}s_W^4\right) \frac{G_F^2 m_Z^4 m_h}{16\pi^3} F\left(\frac{m_Z^2}{m_h^2}\right), \tag{A9}$$

with the form factor  $F(x)$  is formulated as

$$\begin{aligned}
F(x) &= \frac{x-1}{2x} (2 - 13x + 47x^2) - \frac{3}{2} (1 - 6x + 4x^2) \ln x \\
&\quad + \frac{3(1 - 8x + 20x^2)}{\sqrt{4x-1}} \arccos\left(\frac{3x-1}{2x^{3/2}}\right).
\end{aligned} \tag{A10}$$

- 
- [1] G. Aad et al., (ATLAS Collaboration), **Phys.Lett. B** **716**, 1 (2012).  
[2] S. Chatrchyan et al., (CMS Collaboration), **Phys.Lett. B** **716**, 30 (2012).  
[3] G. Aad et al., (ATLAS Collaboration), **Phys.Lett. B** **726**, 120 (2013).  
[4] A. De Roeck, for CMS Collaboration, talk given at LP 2013, June 24-29, 2013, San Francisco, CA, USA.  
[5] G. Aad et al., (ATLAS Collaboration), **Phys.Lett. B** **726**, 88 (2013).  
[6] K. Jakobs, for ATLAS Collaboration, talk given at LP 2013, June 24-29, 2013, San Francisco, CA, USA.  
[7] Z. Chacko, H.-S. Goh and R. Harnik, **Phys.Rev.Lett.** **96**, 231802 (2006); Z. Chacko, Y. Nomura, M. Papucci and G. Perez, **J. High Energy Phys.** **0601**, 126 (2006); A. Falkowski, S. Pokorski and M. Schmaltz, **Phys.Rev. D** **74**, 035003 (2006); R. Foot, R.R. Volkas, **Phys.Lett. B** **645**, 75 (2007).

- [8] Z. Chacko, H.-S. Goh and R. Harnik, **J. High Energy Phys.** **0601**, 108 (2006).
- [9] N. Arkani-Hamed, A. G. Cohen and H. Georgi, **Phys.Lett. B** **513**, 232 (2001); N. Arkani-Hamed, A. G. Cohen, T. Gregoire and J. G. Wacker, **J. High Energy Phys.** **0208**, 020 (2002); N. Arkani-Hamed, A. G. Cohen, E. Katz and A. E. Nelson, **J. High Energy Phys.** **0207**, 034 (2002); I. Low, W. Skiba and D. Smith, **Phys.Rev. D** **66**, 072001 (2002); D. E. Kaplan and M. Schmaltz, **J. High Energy Phys.** **0310**, 039 (2003); S. Chang and J. G. Wacker, **Phys.Rev. D** **69**, 035002 (2004); W. Skiba and J. Terning, **Phys.Rev. D** **68**, 075001 (2003); S. Chang, **J. High Energy Phys.** **0312**, 057 (2003); T. Han, H. E. Logan, B. McElrath and L. T. Wang, **Phys.Rev. D** **67**, 095004 (2003).
- [10] H.-S. Goh and S. Su, **Phys.Rev. D** **75**, 075010 (2007).
- [11] H.-S. Goh and C. A. Krenke, **Phys.Rev. D** **76**, 115018 (2007); **Phys.Rev. D** **81**, 055008 (2010). A. Abada and I. Hidalgo, **Phys.Rev. D** **77**, 113013 (2008); W. Ma, C.-X. Yue and Y.-Z. Wang, **Phys.Rev. D** **79**, 095010 (2009); Y.-B. Liu and X.-L. Wang, **Nucl.Phys. B** **839**, 294 (2010); Y.-B. Liu, **Phys.Lett. B** **698**, 157 (2011).
- [12] E. M. Dolle and S. Su, **Phys.Rev. D** **77**, 075013 (2008).
- [13] M. Carena, S. Gori, N.R. Shah and C.E. Wagner, **J. High Energy Phys.** **1203**, 014 (2012); L. Basso and F. Staub, **Phys.Rev. D** **87**, 015011 (2013); G.F. Giudice, P. Paradisi, A. Strumia, **J. High Energy Phys.** **1210**, 186 (2012); J. Cao et al., **J. High Energy Phys.** **1210**, 079 (2012); **J. High Energy Phys.** **1203**, 086 (2012); J. Cao, Z. Heng, D. Li and J. M. Yang, **Phys.Lett. B** **710**, 665 (2012); U. Ellwanger, **J. High Energy Phys.** **1203**, 044 (2012); A. Arbey, M. Battaglia, A. Djouadi et al., **J. High Energy Phys.** **1209**, 107 (2012); K. Hagiwara, J. S. Lee, J. Nakamura, **J. High Energy Phys.** **1210**, 002 (2012); N. Christensen, T. Han, S. Su, **Phys.Rev. D** **85**, 115018 (2012); B. Kyae, J.-C. Park, **Phys.Rev. D** **87**, 075021 (2013); H. An, T. Liu, L.-T. Wang, **Phys.Rev. D** **86**, 075030 (2012); K. Choi, et al., **J. High Energy Phys.** **1302**, 090 (2013); M. Berg, I. Buchberger, D.M. Ghilencea, C. Petersson, **Phys.Rev. D** **88**, 025017 (2013); L. Aparicio, P.G. Camara, D.G. Cerdeno et al., **J. High Energy Phys.** **1302**, 084 (2013); C. Balazs, S. K. Gupta, **Phys.Rev. D** **87**, 035023 (2013); K. Cheung, C.-T. Lu, T.-C. Yuan, **Phys.Rev. D** **87**, 075001 (2013); W.-Z. Feng, P. Nath, **Phys.Rev. D** **87**, 075018 (2013); R. Nevzorov, S. Pakvasa, [arXiv:1308.1021](https://arxiv.org/abs/1308.1021) [hep-ph]; B. Batell, S. Jung, C.E.M. Wagner, [arXiv:1309.2297](https://arxiv.org/abs/1309.2297) [hep-ph]; J. Huang, T. Liu, L.-T. Wang et al., [arXiv:1309.6633](https://arxiv.org/abs/1309.6633) [hep-ph].
- [14] G. Burdman, C. E. F. Haluch, R. D. Matheus, **Phys.Rev. D** **85**, 095016 (2012); X.-G. He, B. Ren, J. Tandean, **Phys.Rev. D** **85**, 093019 (2012); E. Cervero and J.-M. Gerard, **Phys.Lett. B** **712**, 255 (2012); L. Wang, X.-F. Han, **J. High Energy Phys.** **1205**, 088 (2012); A. Drozd et al., **J. High Energy Phys.** **1305**, 072 (2013); S. Chang et al., **J. High Energy Phys.** **1305**, 075 (2013); N. Chen, H.-J. He, **J. High Energy Phys.** **1204**, 062 (2012); T. Abe, N. Chen, H.-J. He, **J. High Energy Phys.** **1301**, 082 (2013); B. Coleppa, F. Kling, S. Su, [arXiv:1305.0002](https://arxiv.org/abs/1305.0002) [hep-ph]; J. Shu and Y. Zhang, **Phys.Rev.Lett.** **111**, 091801 (2013).
- [15] A. G. Akeroyd, S. Moretti, **Phys.Rev. D** **86**, 035015 (2012); A. Arhrib, R. Benbrik, M. Chabab et al., **J. High Energy Phys.** **1204**, 136 (2012); L. Wang and X.-F. Han, **Phys.Rev. D** **86**, 095007 (2012); **Phys.Rev. D** **87**, 015015 (2013).
- [16] K. Cheung, T.-C. Yuan, **Phys.Rev.Lett.** **108**, 141602 (2012); B. Dumont, S. Fichet, G. Gersdorff, **J. High Energy Phys.** **1307**, 065 (2013); T. Flacke, K. Kong, S.C. Park, [arXiv: 1309.7077](https://arxiv.org/abs/1309.7077) [hep-ph].
- [17] T. Han, H. E. Logan, B. McElrath and L.-T. Wang, **Phys.Lett. B** **563**, 191 (2003); H. E. Logan, **Phys.Rev. D** **70**, 115003 (2004); J. Reuter and M. Tonini, **J. High Energy Phys.** **1302**, 077 (2013); J. Reuter, M. Tonini, M. de Vries, [arXiv:1307.5010](https://arxiv.org/abs/1307.5010) [hep-ph]; [arXiv:1310.2918](https://arxiv.org/abs/1310.2918) [hep-ph].
- [18] A. Arhrib, R. Benbrik, N. Gaur, **Phys.Rev. D** **85**, 095021 (2012); Y. Cai, W. Chao, S. Yang, **J. High Energy Phys.** **1212**, 043 (2012); J. Berger, J. Hubisz, M. Perelstein, **J. High Energy Phys.** **1207**, 016 (2012); S. Dawson, E. Furlan, **Phys.Rev. D** **86**, 015021 (2012).

- [19] A. Goudelis, B. Herrmann, O. Stal, **J. High Energy Phys.** **1309**, 106 (2013); M. Krawczyk, D. Sokolowska, P. Swaczyna, B. Swiezewska, **J. High Energy Phys.** **1309**, 055 (2013); B. Swiezewska, M. Krawczyk, **Phys.Rev. D** **88**, 035019 (2013); D. Bunk, J. Hubisz, B. Jain, [arXiv:1309.7988](#) [hep-ph].
- [20] L. Wang and J. M. Yang, **J. High Energy Phys.** **1005**, 024 (2010); Y.-B. Liu and X.-L. Wang, *Europhys. Lett.* **86**, 61002 (2009); **Phys.Lett. B** **694**, 417 (2011).
- [21] S. Heinemeyer et al., [LHC Higgs Cross Section Working Group], [arXiv:1307.1347](#) [hep-ph].
- [22] J. Beringer et al., [Particle Data Group collaboration], **Phys.Rev. D** **86**, 010001 (2012).
- [23] R.V. Harlander and W.B. Kilgore, **Phys.Rev.Lett.** **88**, 201801 (2002); C. Anastasiou and K. Melnikov, **Nucl.Phys. B** **646**, 220 (2002); V. Ravindran, J. Smith, and W.L. van Neerven, **Nucl.Phys. B** **665**, 325 (2003).
- [24] S. Dittmaier et al., LHC Higgs Cross Section Working Group, Handbook of LHC Higgs Cross Sections: 1. Inclusive Observables, CERN-2011-002, [arXiv:1101.0593](#) [hep-ph].
- [25] R.D. Ball et al., **Nucl.Phys. B** **874**, 746 (2013).
- [26] X.F. Han, L. Wang, J.M. Yang, and J. Zhu, **Phys.Rev. D** **87**, 055004 (2013).
- [27] G. Cacciapaglia, A. Deandrea, G.D. La Rochelle and J.B. Flament, **J. High Energy Phys.** **1303**, 029 (2013).
- [28] G. Belanger et al., **J. High Energy Phys.** **1302**, 053 (2013); K. Cheung, J.S. Lee and P.Y. Tseng, **J. High Energy Phys.** **1305**, 134 (2013); A. Celis, V. Ilisie, and A. Pich, **J. High Energy Phys.** **1307**, 053 (2013); F. Boudjema et al., [arXiv:1307.5865](#) [hep-ph].
- [29] The ATLAS Collaboration, ATLAS-CONF-2013-012; ATLAS-CONF-2013-013; ATLAS-CONF-2013-014; ATLAS-CONF-2013-030; ATLAS-CONF-2013-034.
- [30] The CMS Collaboration, CMS-PAS-HIG-12-025; CMS-PAS-HIG-13-001; CMS-PAS-HIG-13-002; CMS-PAS-HIG-13-003; CMS-PAS-HIG-13-004; CMS-PAS-HIG-13-005.
- [31] J.R. Espinosa, C. Grojean, M. Muhlleitner, and M. Trott, **J. High Energy Phys.** **1205**, 097 (2012); **J. High Energy Phys.** **1212**, 045 (2012); P.P. Giardino, K. Kannike, M. Raidal, and A. Strumia, **J. High Energy Phys.** **1206**, 117 (2012); **Phys.Lett. B** **718**, 469 (2012).
- [32] B. Dumont, S. Fichet, and G. Gersdorff, **J. High Energy Phys.** **1307**, 065 (2013).
- [33] S. Dutta, K. Hagiwara, and Y. Matsumoto, **Phys.Rev. D** **78**, 115016 (2008); L. Wang, F. Xu, and J.M. Yang, **J. High Energy Phys.** **1001**, 107 (2010); R. Contino et al., [arXiv:1309.7038](#) [hep-ph]; D.M. Asner et al., [arXiv:1310.0763](#) [hep-ph].
- [34] W.Y. Keung and W.J. Marciano, **Phys.Rev. D** **30** 248 (1984); A. Djouadi, **Phys. Rep.** **457** 1 (2008).